Advances in Geo-Energy Research

Vol. 5, No. 2, p. 202-211, 2021

Original article

Single-phase inflow performance relationship in stress-sensitive reservoirs

Fei Wang[1], Ruxiang Gong[1], Zijun Huang[1], Qingbang Meng[2], Qi Zhang[2]*, Shiyuan Zhan[3,4]

[1]*China Oilfield Services Limited, Tianjin 300452, P. R. China*

[2]*School of Earth Resources, China University of Geoscience, Wuhan 430074, P. R. China*

[3]*School of Petroleum Engineering, China University of Petroleum (East China), Qingdao 266580, P. R. China*

[4]*School of Mining and Petroleum Engineering, University of Alberta, Edmonton, Canada*

Keywords:
Stress-sensitive reservoirs
inflow performance relationship
single phase
reservoir simulation
Vogel-type IPR

Cited as:
Wang, F., Gong, R., Huang, Z., Meng, Q., Zhang, Q., Zhan, S. Single-phase inflow performance relationship in stress-sensitive reservoirs. Advances in Geo-Energy Research, 2021, 5(2): 202-211, doi: 10.46690/ager.2021.02.09

Abstract:
For stress-sensitive reservoirs, understanding the characteristics of the inflow performance relationship is vital for evaluating the performance of a well and designing an optimal stimulation. In this study, a reservoir simulator was used to establish the inflow performance relationship of a well for a wide variety of reservoirs and wellbore conditions. First, a base case was simulated using typical reservoir, wellbore, and fluid parameters. Subsequently, variations from the base case were investigated. The results of the simulation indicate that the dimensionless inflow performance relationship in the stress-sensitive reservoir is similar to the Vogel-type inflow performance relationship, which is used for evaluating the productivity of a vertical well in a solution-gas-drive reservoir. Unlike the two-phase flow in a solution-gas-drive reservoir, the nonlinear characteristic of the inflow performance relationship in stress-sensitive reservoirs is caused by stress-dependent permeability. Furthermore, the stress sensitivity level is the only parameter that affects the nonlinearity coefficient of the dimensionless inflow performance relationship equation. The nonlinearity coefficient was plotted against the stress sensitivity index, and the nonlinearity coefficient was found to be linearly proportional to the stress sensitivity index. This study provides a realistic and less expensive methodology to evaluate the reservoir productivity of stress-sensitive reservoirs when the reservoir stress sensitivity level is known and to predict the reservoir stress sensitivity level when the inflow performance relationship of the stress-sensitive reservoirs is known.

1. Introduction

Reservoir productivity is affected by various factors, such as absolute permeability, pay thickness, drainage area, and wellbore properties. In general, the effect of absolute permeability is considered to be unchanged with changes in the pore pressure and stress state. However, for some reservoirs, particularly tight reservoirs, the absolute permeability can change significantly with varying pore pressure and stress state (Fatt et al., 1952; McLatchie et al., 1958; Jennings et al., 1981; Jones, 1988; Choi et al., 2008). This phenomenon is called "stress sensitivity" or "stress-dependent permeability". In stress-sensitive reservoirs, reservoir depressurization can increase the net effective stress, which changes the bearing skeletons, solid particles, and pore throats of porous media (Fatt, 1958; Vogel, 1968). It has been reported that significant stress sensitivity causes a sharp decline in the production rate, low recovery, and major financial losses during depletion (Lei et al., 2015; Li et al., 2019; Han and Bartko, 2020; Tan et al., 2021). The greatest pressure drop occurs within a short distance from the wellbore; thus, the net effective stress is highest near the wellbore, resulting in the greatest reduction in absolute permeability (Abass et al., 2007).

The study of the inflow performance relationship (IPR) in stress-sensitive reservoirs is significant for designing optimal stimulation treatments and predicting reservoir performance. Lei et al. (2015) developed a deliverability equation that considers the stress sensitivity, and the results showed that the stress sensitivity has an effect on both the permeability

Yandy Scientific Press

*Corresponding author.
E-mail address: wangfei11@cosl.com.cn (F. Wang); gongrx@cosl.com.cn (R. Gong); huangzj3@cosl.com.cn (Z. Huang); mengqb@cug.edu.cn (Q. Meng); qizhang@cug.edu.cn (Q. Zhang); zhangshiyuan321@163.com (S. Zhan).

Received March 1, 2021; revised March 23, 2021; accepted March 24, 2021; available online March 28, 2021.

near wells and the production rate of stress-sensitive reservoirs. A numerical model that simulates single-phase flow through a deforming porous medium with stress sensitivity was developed by Raghavan et al. (1999) to calculate the reservoir productivity with variations in wellbore properties. The simulation results indicated that the loss in productivity was influenced only by Poisson's ratio in stress-sensitive reservoirs. Davies et al. (1999) investigated the stress sensitivity in unconsolidated, high-porosity sand reservoirs and reservoirs with moderate to low consolidation, including tight gas sands. Furthermore, a practical methodology was developed to improve the evaluation and enhance the productivity and management of stress-sensitive reservoirs. Osorio et al. (1999) developed a 3-D finite-difference, fully implicit model that considers two different physical domains to simulate the physical phenomena in stress-sensitive reservoirs. The model was applied to illustrate the effect of rock deformation on reservoir productivity, and the results of the simulation showed that the production rates calculated from coupled, single-domain models can differ from the production rates calculated from fully coupled, two-domain models. However, the method used to evaluate reservoir productivity in the stress-sensitive reservoirs discussed above is complicated and time consuming.

In stress-sensitive reservoirs, the absolute permeability of rocks can change with the variation of the pore pressure and stress state, which has a significant impact on reservoir productivity. Understanding the characteristics of the IPR (Huang et al., 1995; Jahanbani and Shadizadeh, 2009; Qasem et al., 2014; Changalvaie et al., 2015; Youssef, 2019; Zhang et al., 2020) is vital for evaluating the performance of a well and designing an optimal stimulation. The primary objective of this study was to provide a rapid and cost-efficient methodology to evaluate reservoir productivity in stress-sensitive reservoirs. In this study, a reservoir simulator (Eclipse) was utilized to construct the IPRs of stress-sensitive reservoirs. First, a base case was considered with typical reservoir, wellbore, and fluid properties. The inflow performance relationship was used to describe the relationship between the flowing bottom-hole pressure (P_{wf}) of the well and flow rate (Q_o) at a stabilized reservoir pressure. Then, variations of the base case were investigated, and the IPRs for all of the reservoirs were constructed. When the IPRs of reservoirs with different stress sensitivity levels are obtained, they can be used to evaluate the productivity of wells quickly but accurately and enable petroleum engineers to optimize production design and predict recovery for project planning.

2. Description of the base case reservoir

The base case was modeled as a box-shaped reservoir with a square drainage area of 26×10^4 m^3 and a constant thickness of 20 m. Its dimensions were $17\times17\times20$ in the simulation, i.e., there were 17 grid blocks in the X direction, 17 grid blocks in the Y direction, and 20 grid blocks in the Z direction. The reservoir had a homogeneous porosity of 0.139 and an isotropic absolute permeability of 1×10^{-3} μm^2. The vertical-to-horizontal permeability ratio was 0.1, and the stress sensitivity level is defined as follows (Liu et al., 2000).

$$K = K_o e^{-b(P_o-P)} \tag{1}$$

where K_o is the permeability at the initial reservoir pressure (m^2), b is the stress sensitivity index (MPa^{-1}), P_o is the initial reservoir pressure (MPa), and P is the pore pressure of the rock (MPa). In the base case reservoirs, the stress sensitivity index was 0.05 MPa^{-1}, and the initial reservoir pressure was 30 MPa, as shown in Table 1. A horizontal well with zero skin factor was located in the middle of the reservoir, and the length of the well was 480 m, as shown in Fig. 1. To maintain the reservoir pressure at the reservoir boundaries, an aquifer was added. The oil viscosity was 3 mPa·s, and the oil density was 800 kg/m^3.

Table 1. Permeability curves under different pore pressures.

P/MPa	K/K_o
0.01	0.23
0.50	0.24
2.00	0.28
4.00	0.35
6.00	0.42
8.00	0.52
10.00	0.63
12.00	0.77
14.00	0.94
14.59	1.00

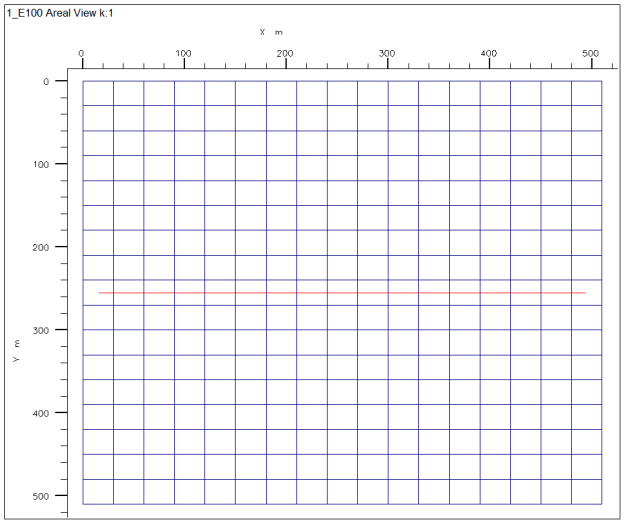

Fig. 1. Schematic Diagrams for the basic model in this work.

3. Procedure for obtaining IPRs

An IPR curve is generated by obtaining a series of points relating flowing bottom-hole pressures to the production rate. For each run, the corresponding reservoir and wellbore parameters are fed into the reservoir simulator, and a series of inflow points are simulated. The IPR curve of each case is generated using 16 different bottom-hole pressures ranging from 0 to 30 MPa. At the initial stage of the simulation, the production rate declines rapidly because the pressure wave

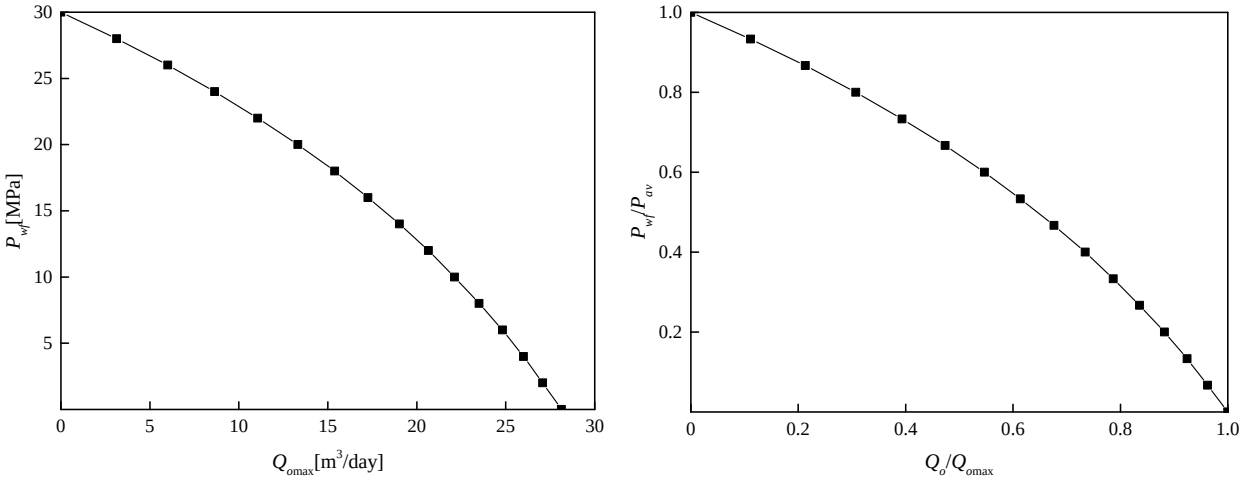

(a) IPR in base case reservoir

(b) dimensionless IPR in base case reservoir

Fig. 2. IPR and dimensionless IPR curves in the base case reservoir.

does not transfer to the reservoir boundary. In this study, the flow rate of the production well was recorded when the production rate remained almost constant. The IPRs were obtained by plotting the flowing bottom-hole pressures (P_{wf}) versus the production rate (Q_o), and the dimensionless IPRs were obtained by plotting $Q/Q_{o\max}$ versus P_{wf}/P_{av}. In this study, $Q_{o\max}$ and P_{av} were the maximum production rate and initial reservoir pressure, respectively.

Fig. 2 shows the single-phase IPR and dimensionless IPR of the base case. Fig. 2 shows that the single-phase IPR in a stress-sensitive reservoir is nonlinear and similar to the Vogel-type IPR in a solution-gas-drive reservoir (Liu et al., 2000; Zeng et al., 2005; Ren et al., 2017). For a solution-gas-drive reservoir, in the early stage of reservoir depletion, the IPR decreases sharply with the reservoir depletion. With a decrease in reservoir pressure, the IPR curve rapidly deviates to the flow pressure axis. In addition, in the late stage of reservoir depletion, the IPR decreases slowly. However, in contrast to the result of two-phase flow, the nonlinear characteristic of the single-phase IPR in stress sensitivity is caused by stress-dependent permeability. When the bottom-hole pressure is low, the decline of the absolute permeability is large, and the decrease in the production rate is large compared with a reservoir without stress sensitivity. When the bottom-hole pressure is high, the decline of the absolute permeability is small, and the decrease in the production rate is small compared with the reservoir without stress sensitivity.

For the IPR curve obtained from the simulation, a curve fitting was performed in which a generalized Vogel-type relationship was fitted to the curve (Vogel, 1968). The IPR curve of the base case can be described by the following equation (Bendakhlia and Aziz, 1989; Liu et al., 2012).

$$\frac{Q_o}{Q_{o\max}} = 1 - 0.4137\left(\frac{P_{wf}}{P_{av}}\right) - 0.5863\left(\frac{P_{wf}}{P_{av}}\right)^2 \qquad (2)$$

where Q_o is the production rate (m^3/d), P_{wf} is the flowing bottom-hole pressure (MPa), $Q_{o\max}$ is the maximum production rate at the maximum drawdown or at zero bottom-hole flowing pressure for single-phase oil flow (m^3/d), P_{av} is the initial reservoir pressure (MPa), and 0.4137 is the fitting parameter.

4. Interpretation of the results

4.1 Effect of reservoir parameters

The reservoir parameters include absolute permeability, porosity, vertical-to-horizontal permeability ratio, pay thickness, drainage area, reservoir heterogeneity degree, and stress sensitivity level. The effects of these parameters on the IPR curves were analyzed. The unnormalized IPR is useful for visualizing the production behavior of a well. The effect of absolute permeability on the production behavior is shown in Figs. 3(a) and (b). The production rate increases rapidly with an increase in the absolute permeability, as shown in Fig. 3(a). This means that a larger reservoir absolute permeability causes higher production under the same pressure drop. However, the shape of the dimensionless IPRs shows no significant change with an increase in the absolute permeability, as shown in Fig. 3(b). The effect of porosity on the IPR curves is shown in Figs. 3(c) and (d). Similar to the effect of the absolute permeability, the production rate increases with the increase in porosity, which means that a larger porosity of the reservoir leads to higher production under the same pressure drop, as shown in Fig. 3(c). The dimensionless IPRs do not change significantly, as shown in Fig. 3(d).

The effect of the vertical-to-horizontal permeability ratio on the IPR curves is shown in Figs. 4(a) and (b). The production rate increases as the vertical-to-horizontal ratio increases, which means that stronger heterogeneity causes lower production under the same pressure drop, as shown in Fig. 4(a). The dimensionless IPRs showed no significant change, as shown in Fig. 4(b). The effects of pay thickness on the IPR curves are presented in Figs. 4(c) and (d). A large pay thickness indicates a large productivity potential. Hence, the production rate increases with an increase in pay thickness, as

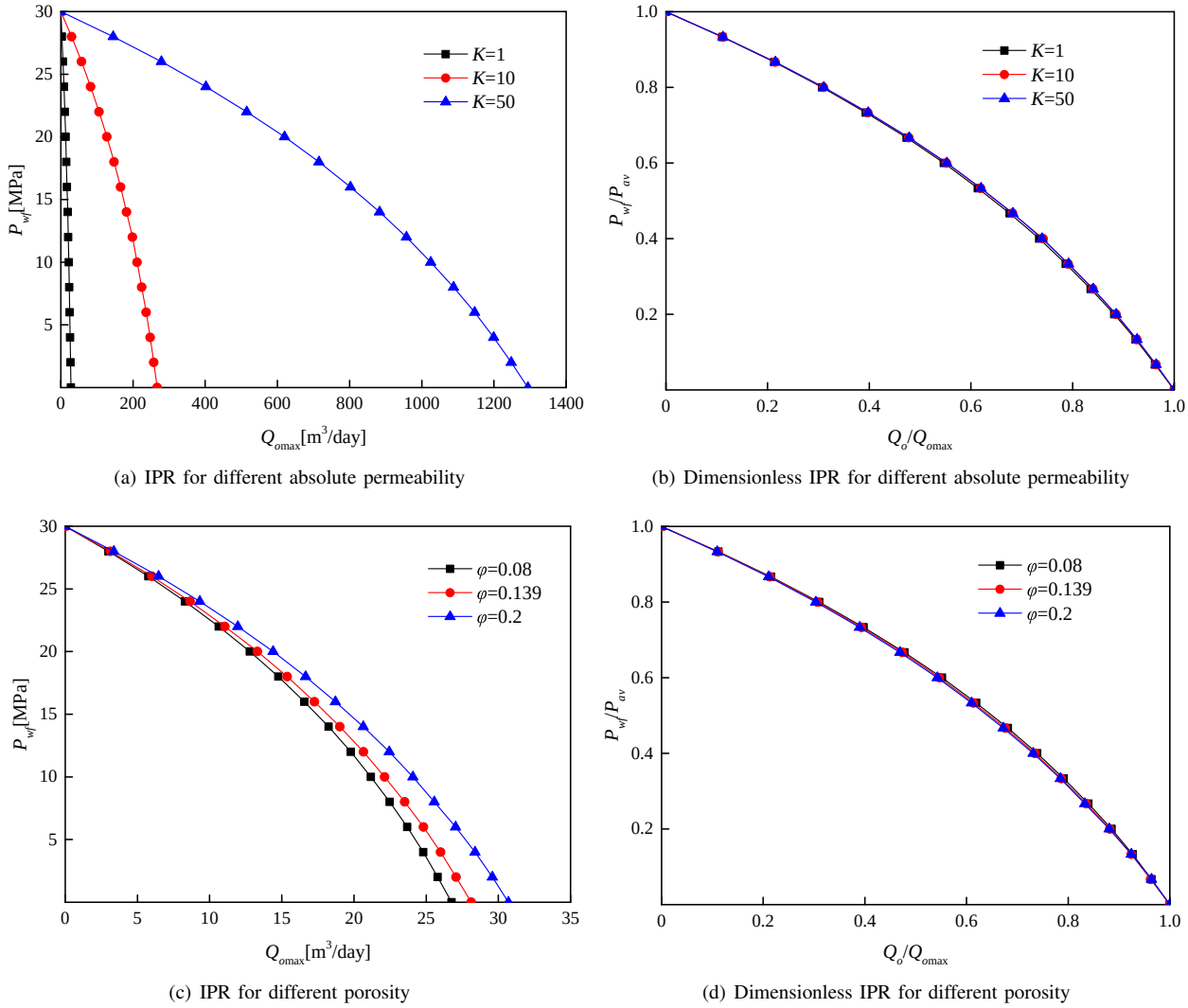

(a) IPR for different absolute permeability

(b) Dimensionless IPR for different absolute permeability

(c) IPR for different porosity

(d) Dimensionless IPR for different porosity

Fig. 3. The effects of absolute permeability and porosity on IPR and dimensionless IPR curves.

shown in Fig. 4(c). The dimensionless IPRs also showed no significant change, as shown in Fig. 4(d).

The effect of the drainage area on the IPR curves is shown in Figs. 5(a) and (b). The production rate decreases with the increase in drainage area, as shown in Fig. 5(a), because the increasing drainage radius results in a decrease in the pressure gradient. However, the shape of the dimensionless IPRs does not change significantly, as shown in Fig. 5(b). The effect of the degree of reservoir heterogeneity on the IPR curves is shown in Figs. 5(c) and (d). The reservoir heterogeneity degree is described by the Lorentz coefficient (V_k). The reservoir heterogeneity degree increases with an increase in the Lorentz coefficient. The simulation results show that the production rate decreases with an increase in the Lorentz coefficient, as shown in Fig. 5(c). However, the shape of the dimensionless IPRs does not change significantly, as shown in Fig. 5(d).

The effect of the stress sensitivity level on the IPR curves is shown in Figs. 6(a) and (b). The stress sensitivity level is given by Eq. (1). The stress sensitivity level increased with an increase in the stress sensitivity index. The simulation results show that the single-phase IPR is linear, and the production rate is high when the stress sensitivity index is zero. The single-phase IPRs are nonlinear when the stress sensitivity index is not zero, and the production rate decreases with an increase in the stress sensitivity level, as shown in Fig. 6(a). Furthermore, the dimensionless IPRs change significantly for different stress sensitivity indices, and the curvature of the IPR increases with an increase in the stress sensitivity index, as shown in Fig. 6(b).

4.2 Effect of wellbore parameters

The other important parameters are wellbore parameters, including skin, well location, and well length with respect to the reservoir boundary. The effects of these parameters on the IPR curves were analyzed. The effect of the skin factor on the IPR curves is shown in Figs. 7(a) and (b). The production rate decreases with an increase in the skin factor, as depicted in Fig. 7(a), because the resistance of the wellbore increases. However, the dimensionless IPRs do not change significantly for the different skin factors, as shown in Fig. 7(b). In addition,

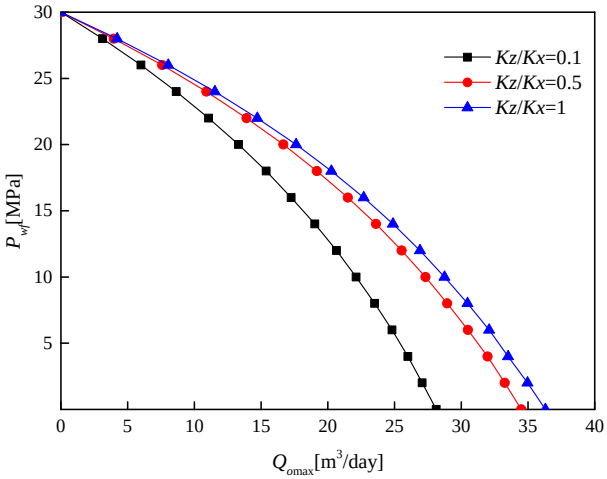

(a) IPR for different vertical to horizontal permeability ratio

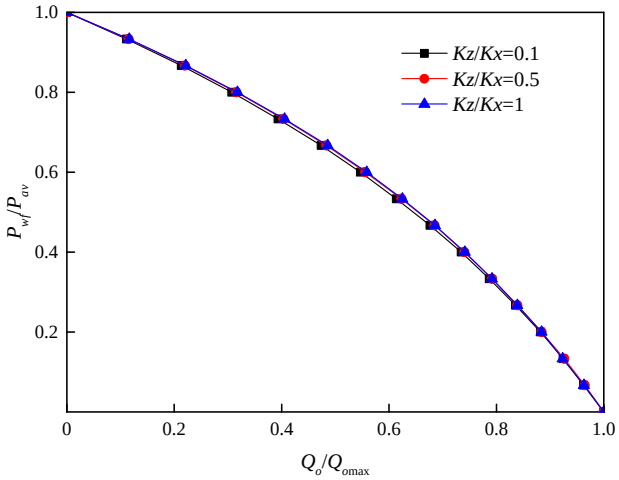

(b) Dimensionless IPR for different vertical to horizontal permeability ratio

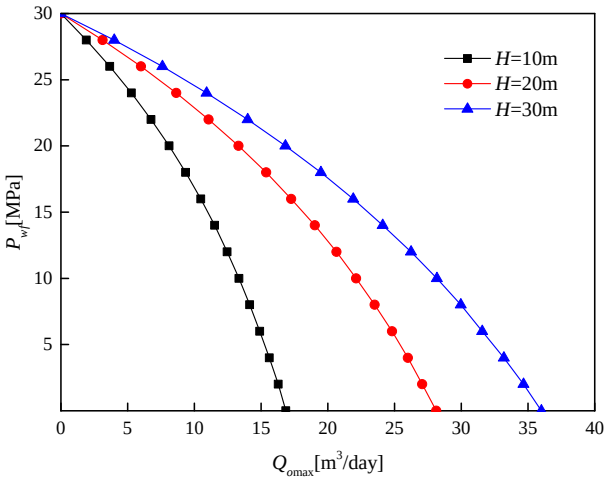

(c) IPR for different pay thickness

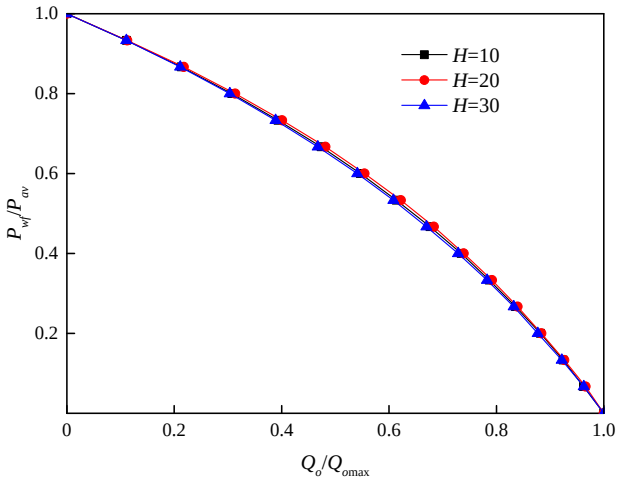

(d) Dimensionless IPR for different pay thickness

Fig. 4. The effects of vertical to horizontal permeability ratio and pay thickness on IPR and dimensionless IPR curves.

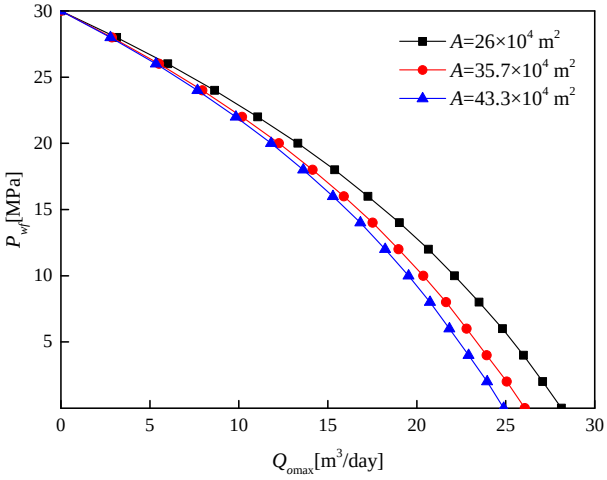

(a) IPR for different drainage area

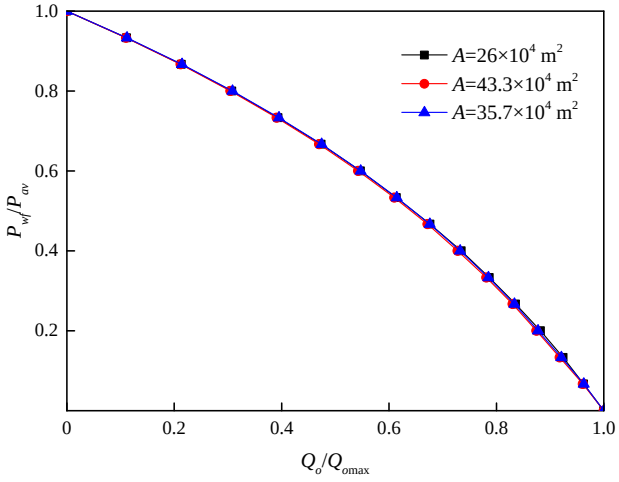

(b) Dimensionless IPR for different drainage area

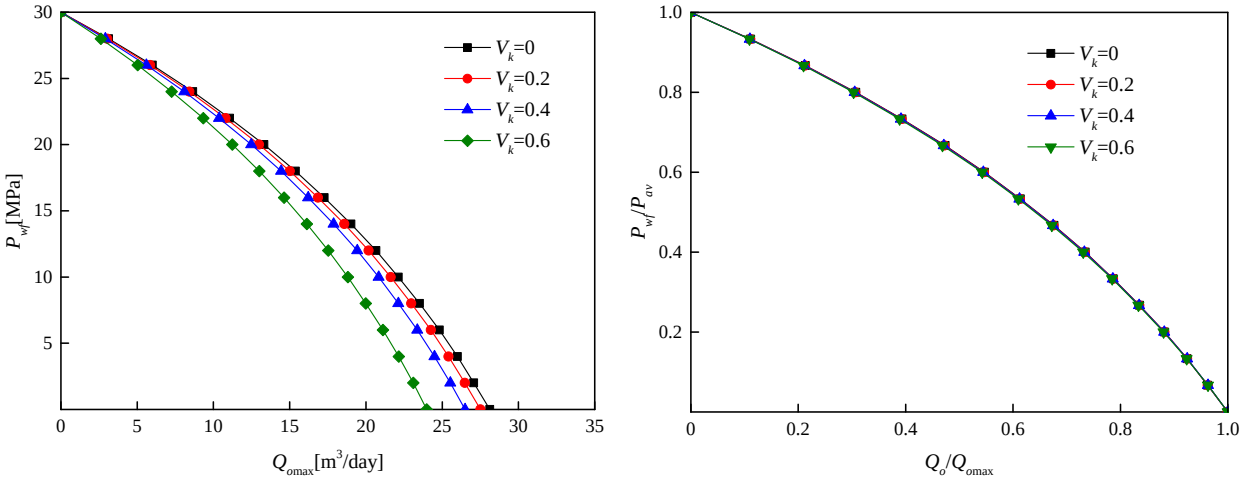

(c) IPR for different reservoir heterogeneous degree (d) Dimensionless IPR for different reservoir heterogeneous degree

Fig. 5. The effects of drainage area and reservoir heterogeneous degree on IPR and dimensionless IPR curves.

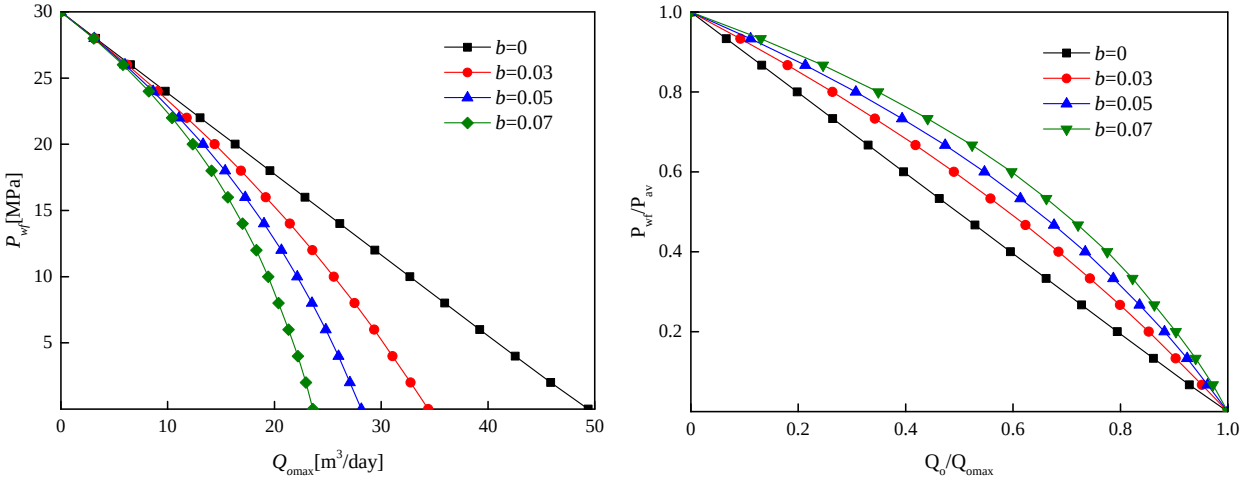

(a) IPR for different stress sensitivity level (b) Dimensionless IPR for different stress sensitivity level

Fig. 6. The effect of stress sensitivity level on IPR curves.

the effect of the well location on the IPR curves is shown in Figs. 7(c) and (d). The production rate does not change significantly when the well is located at the top or bottom of the reservoir. However, the production rate is higher when the well is located in the middle of the reservoir, as shown in Fig. 7(c), which indicates that the well location in the middle of the reservoir can develop more oil in the reservoir under the same pressure drop. Similarly, the dimensionless IPR curves do not change significantly for different well locations, as shown in Fig. 7(d).

The effect of well length with respect to the reservoir boundary on the IPR curves is shown in Figs. 8(a) and (b). The production rate increases with the increase in well length because a longer well length leads to a larger drainage area and larger production under the same pressure drop, as shown in Fig. 8(a). However, the dimensionless IPR curves do not change significantly for different well lengths, as shown in Fig. 8(b).

4.3 Effect of fluid parameters

The fluid parameters also have significant effects on the IPR curves, especially the fluid viscosity. Because this study focused on single-phase flow, the only fluid parameter that can significantly impact the production rate is the oil viscosity. The effect of oil viscosity on the IPR curves is shown in Figs. 9(a) and (b). The production rate decreases rapidly with the increase in oil viscosity because the high oil viscosity causes a rapid increase in the flow resistance in the reservoir, as shown in Fig. 9(a). However, the dimensionless IPR curves show no significant change for different oil viscosities, as shown in Fig. 9(b).

4.4 IPR curve fitting

Because the curvature of the IPR increases with an increase in the stress sensitivity level, an attempt was made to correlate these changes with a modified form of Vogel-type IPR (Vogel, 1968). The modified form of the Vogel-type IPR equation is

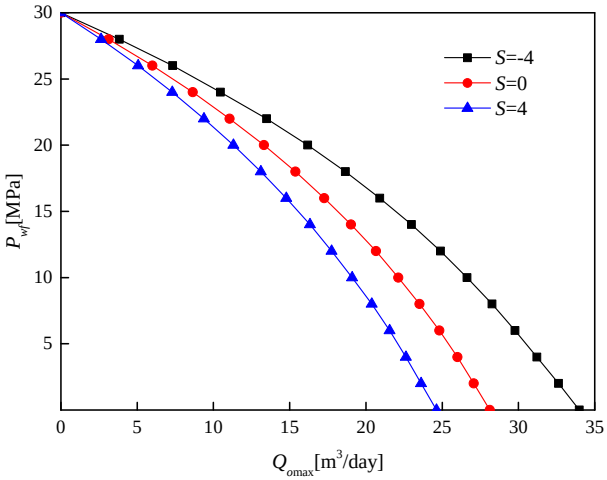

(a) IPR for different skin factors

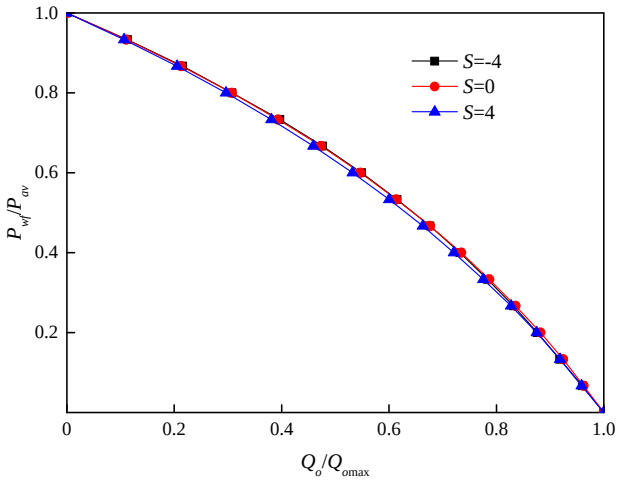

(b) Dimensionless IPR for different skin factors

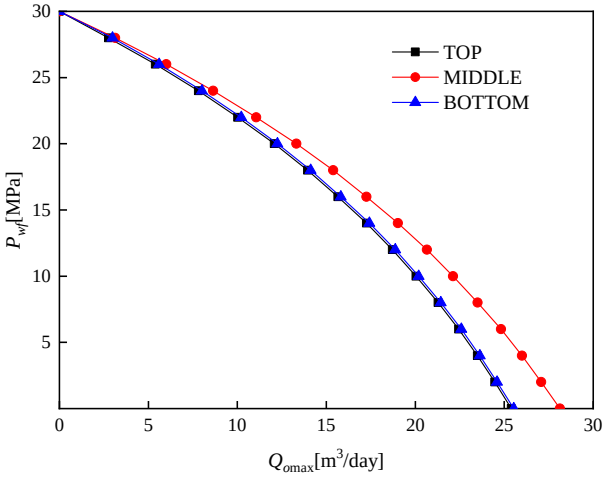

(c) IPR for different well location

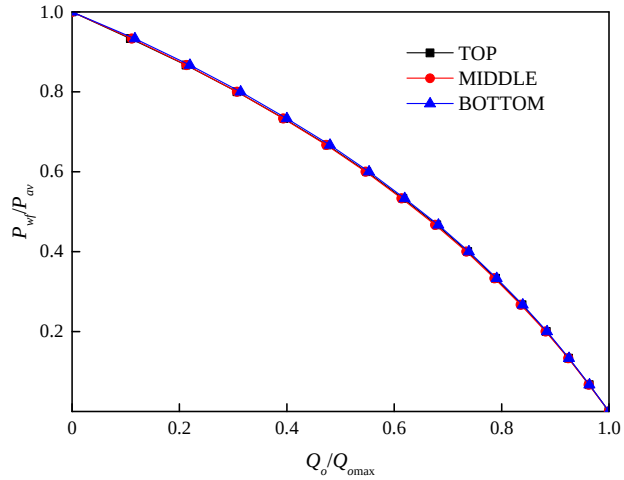

(d) Dimensionless IPR for different well location

Fig. 7. The effects of skin factors and well location on IPR and dimensionless IPR curves.

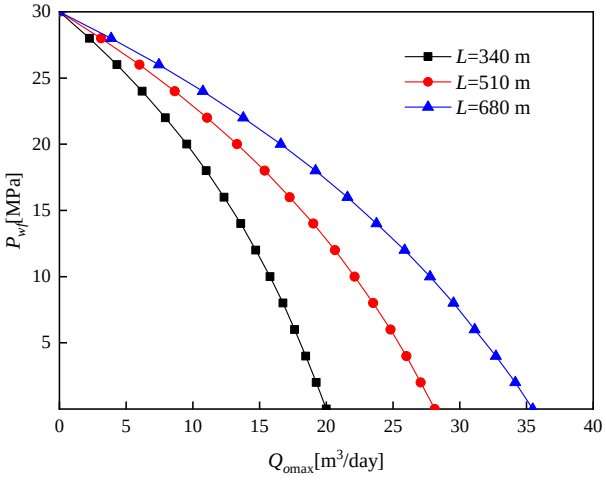

(a) IPR for different well length

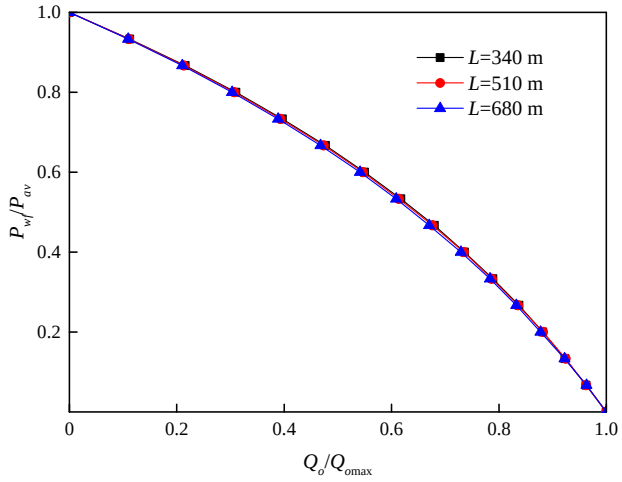

(b) Dimensionless IPR for different well length

Fig. 8. The effect of well length on IPR curves.

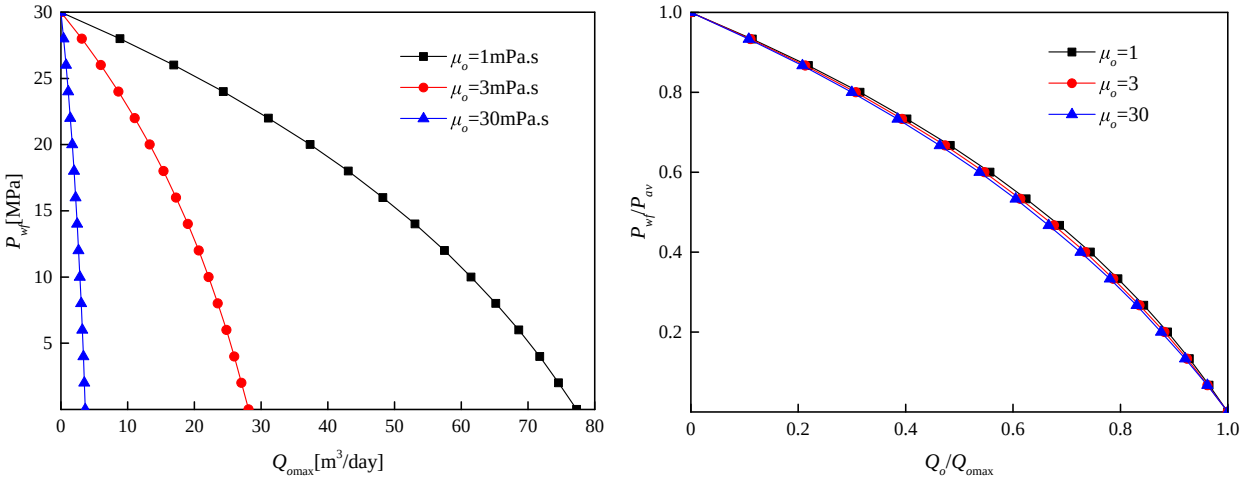

(a) IPR for different oil viscosity

(b) Dimensionless IPR for different oil viscosity

Fig. 9. The effect of oil viscosity on IPR curves.

given by

$$\frac{Q_o}{Q_{o\max}} = 1 - V\left(\frac{P_{wf}}{P_{av}}\right) - (1-V)\left(\frac{P_{wf}}{P_{av}}\right)^2 \qquad (3)$$

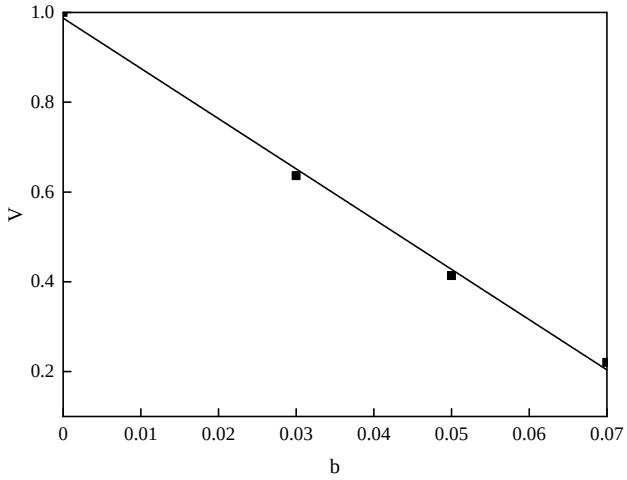

Fig. 10. Plots of the nonlinear coefficient versus the stress sensitivity index.

where V is the dimensionless nonlinearity coefficient. Eq. (3) is quite similar to Vogel's equation, but the mechanisms are different. The nonlinearity of Vogel's equation in a vertical well is caused by the effect of two-phase (oil and gas) flow (Vogel, 1968; Kamkom and Zhu, 2005; Yao et al., 2008; Liu et al., 2013; He et al., 2019; Salam, 2019), whereas the nonlinearity of Eq. (3) is mainly caused by the stress sensitivity.

This equation was fitted to the dimensionless IPR curves for different stress sensitivity levels, as shown in Table 2. Table 2 shows a comparison of the curves fitted by Eq. (3) and the actual ones. Eq. (3) gives a close fit to the actual IPR values, especially for the weak stress sensitivity level. The nonlinear coefficient of the IPR curves was plotted against the stress sensitivity index, revealing that the nonlinearity coefficient is linear with the stress sensitivity index (Fig. 10).

5. Conclusions

In this study, single-phase IPRs in stress-sensitive reservoirs were constructed, and the effects of the reservoir, wellbore, and fluid property parameters on the IPRs were investigated. The results of the simulation show that the only factor that affects the IPR is the stress sensitivity level. Therefore, if the stress sensitivity level is known, reservoir productivity can be evaluated quickly and accurately using Vogel-type IPRs. Furthermore, according to the results of this study, there is another significant function for the Vogel-type IPR. A review of the literature revealed that the stress sensitivity phenomenon was first reported in the laboratory. Traditionally, it has been recognized that the stress sensitivity level is high, particularly in tight sandstone. However, there is no methodology for estimating the stress sensitivity level in the formation condition. The IPR can be used to evaluate the stress sensitivity level under the formation condition. In this study, a reservoir simulator was used to construct IPRs in stress-sensitive reservoirs. Based on the simulation results, the following conclusions were drawn.

1) The single-phase IPR in stress-sensitive reservoirs is nonlinear, resulting from the stress-dependent permeability, which is similar to the Vogel-type IPR in a solution-gas-drive reservoir. However, unlike the results of two-phase

Table 2. Comparison between the fitted curves and the actual ones.

$b=0$				$b=0.03$			
Q_o/Q_{max}	Actual values	Fitting values	Error %	Q_o/Q_{max}	Actual values	Fitting values	Error %
1	0	0	0	1	0	0	0
0.929	0.067	0.067	0.000	0.952	0.067	0.064	3.288
0.794	0.200	0.200	0.000	0.853	0.200	0.193	3.528
0.662	0.333	0.333	0.000	0.743	0.333	0.326	2.122
0.529	0.467	0.467	0.000	0.623	0.467	0.462	0.942
0.397	0.600	0.600	0.000	0.490	0.600	0.601	-0.127
0.264	0.733	0.733	0.000	0.343	0.733	0.739	-0.778
0.132	0.867	0.867	0.000	0.180	0.867	0.874	-0.790
0	1	1	0	0	1	1	0
$b=0.05$				$b=0.07$			
Q_o/Q_{max}	Actual values	Fitting values	Error %	Q_o/Q_{max}	Actual values	Fitting values	Error %
1	0	0	0	1	0	0	0
0.962	0.067	0.059	11.942	0.972	0.067	0.049	27.063
0.882	0.200	0.179	10.693	0.904	0.200	0.164	17.764
0.787	0.333	0.312	6.470	0.823	0.333	0.291	12.708
0.676	0.467	0.452	3.169	0.721	0.467	0.436	6.604
0.547	0.600	0.598	0.266	0.598	0.600	0.590	1.672
0.393	0.733	0.746	-1.788	0.441	0.733	0.751	-2.449
0.213	0.867	0.885	-2.118	0.246	0.867	0.898	-3.665
0	1	1	0	0	1	1	0

flow, the nonlinear characteristics of the single-phase IPR in stress sensitivity are caused by stress-dependent permeability.

2) The factors influencing the IPR curves, including the reservoir parameters, wellbore parameters, and fluid parameters, were studied. The only factor that affects the single-phase dimensionless IPR in stress-sensitive reservoirs is the stress sensitivity level. The nonlinearity coefficient is linear proportional to the stress sensitivity index.

Acknowledgement

The authors would like to give thanks for the National Natural Science Foundation of China (No. 51904279).

Conflict of interest

The authors declare no competing interest.

References

Abass, H. H., Ortiz, I., Khan, M. R., et al. Understanding stress dependant permeability of matrix, natural fractures, and hydraulic fractures in carbonate formations. Paper SPE 110973 Presented at SPE Saudi Arabia Section Technical Symposium, Dhahran, Saudi Arabia, 7 May, 2007.

Bendakhlia, H., Aziz, K. Inflow performance relationships for solution-gas drive horizontal wells. Paper SPE 19823 Presented at the 64th Annual Technical Conference and Exhibition of the Society of Petroleum Engineers, San Antonio, Texas, 8-11 September, 1989.

Changalvaie, A. A., Abdideh, M., Azizi, S. M. Optimum production potentials for gas wells using inflow performance relationships (IPR) curves. Energy Sources Part A-Recovery Utilization and Environmental Effects, 2015, 37(7): 775-780.

Choi, S. K., Ouyang, L. B., Huang, W. S. A Comprehensive comparative study on analytical PI/IPR correlations. Paper SPE 116580 Presented at the SPE Annual Technical Conference and Exhibition, Colorado, USA, 21 September, 2008.

Davies, J. P., Davies, D. K. Stress-dependent permeability: characterization and modeling. Paper SPE 56813 Presented at SPE Annual Technical Conference and Exhibition, Houston, Texas, 3-6 October, 1999.

Fatt, I. Pore volume compressibilities of sandstone reservoir rocks. Journal of Petroleum Technology, 1958, 10(3): 64-66.

Fatt, I., Davis, D. H. Reduction in permeability with overburden pressure. Journal of Petroleum Technology, 1952, 4(12): 16.

Han, G., Bartko, K. Study quantifies stress sensitivity of fractured tight reservoirs. Journal of Petroleum Technology, 2020, 72(10): 56-57.

He, C., Fan, Z., Xu, A., et al. Foamy oil properties and horizontal well inflow performance relationship under solution gas drive. Geosystem Engineering, 22(3): 151-160.

Huang, B., Li, S., Zhou, R. An application of IPR curves in the production behavior analysis of a horizontal well. Petroleum Exploration and Development, 1995, 22(5): 56-58.

Jahanbani, A., Shadizadeh, S. R. Determination of inflow performance relationship (IPR) by well testing. Paper Presented at the Canadian International Petroleum Conference, Calgary, Alberta, 16-18 June, 2009.

Jennings, J. B., Carroll, H. B., Raible, C. J. The relationship of permeability to confining pressure in low permeability rock. Paper SPE 9870 Presented at SPE Low Permeability Gas Reservoirs Symposium, Denver, Colorado, 27-29 May, 1981.

Jones, S. C. Two-point determinations of permeability and PV vs. Net Confining Stress. SPE Formation Evaluation, 1988, 3(1): 235-241.

Kamkom, R., Zhu, D. Evaluation of two-phase IPR correlations for horizontal wells. Paper SPE 93986 Presented at SPE Production and Operations Symposium, Oklahoma, USA, 16-19 April, 2005.

Lei, G., Wu, Z., Gai, S., et al. A fractal model for the stress-dependent permeability and relative permeability in tight sandstones. Journal of Canadian Petroleum Technology, 2015, 54(1): 36-48.

Li, B., Zhou, F., Fan, W., et al. Experimental investigation and theoretical modeling of stress-dependent permeability in naturally fractured tight gas reservoir. Journal of Petroleum Science and Engineering, 2020, 188: 106949.

Liu, H., Wang, J., Zheng, J., et al. Single-Phase inflow performance relationship for horizontal, pinnate-branch horizontal, and radial-branch wells. SPE Journal, 2012, 18: 219-232.

Liu, X., Jiang, Z., Liu, X., et al. Numerical simulation of inflow performance relationships for solution gas drive horizontal wells. Acta Petrolel Sinica, 2000, 21(1):60-63. (in Chinese)

McLatchie, A. S., Hemstock, R. A., Young J. W. The effective compressibility of reservoir rock and its effects on permeability. Journal of Petroleum Technology, 1958, 10(6): 49-51.

Osorio, J. G., Chen, H., Teufel, L. W. Numerical simulation of the impact of flow-induced geomechanical response on the productivity of stress-sensitive reservoirs. Paper SPE 51929 Presented at SPE Reservoir Simulation Symposium, Houston, Texas, 14-17 February, 1999.

Raghavan, R., Chin, L. Y. Productivity changes in reservoirs with stress-dependent permeability. Paper SPE 77535 Presented at SPE Annual Technical Conference and Exhibition, Houston, Texas, 26-29 September, 2004.

Ren, Z., Wu, X., Li, H. Inflow performance relationship (IPR) equation for a damaged well in solution-gas drive production. Chemistry and Technology of Fuels and Oils, 2017, 52(6): 736-743.

Salam, A. R. Pseudo-steady state inflow performance relationship of reservoirs undergoing multiphase flow and different well bore conditions. Journal of Natural Gas Science and Engineering, 2019, 68: 102912.

Tan, Q., Kang, Y., You, L., et al. Stress-sensitivity mechanisms and its controlling factors of saline-lacustrine fractured tight carbonate reservoir. Journal of Natural Gas and Engineering, 2021, 88: 103864.

Vogel, J. V. Inflow performance relationships for solution-gas drive wells. Journal of Petroleum Technology, 1968, 20(1): 83-92.

Yao, J., Liu, S., Xu, Y. Establishment of inflow performance relationship of horizontal wells in low-permeability reservoir. Journal of China University of Petroleum (Edition of Natural Science), 2008, 32(4): 64-67+72. (in Chinese)

Youssef, A. A. Inflow performance relationship of vertical wells in fractured vuggy media during semi-steady state flow regime. Journal of Petroleum Science and Engineering, 2019, 176: 970-981.

Zeng, X., He, G., Sun, F., et al. Study on a new IPR curve of horizontal wells in solution gas drive reservoirs. Special Oil and Gas Reservoirs, 2005, 12(4): 47-49. (in Chinese)

Zhang, R., Yin, Y., Xiao, L., et al. Calculation method for inflow performance relationship in sucker rod pump wells based on real-time monitoring dynamometer card. Geofluids, 2020, 2020: 8884988.